PAPER

Check for updates

Non-toxic green food additive enables efficient polymer solar cells through adjusting the phase composition distribution and boosting charge transport†

Jianfeng Li, [iD] ‡*[a] Yufei Wang, [iD] ‡[a] Zezhou Liang, [iD][a] Jicheng Qin,[a] Meiling Ren,[a] Junfeng Tong, [iD][a] Chunyan Yang,[a] Chunming Yang,[b] Xichang Bao [iD] *[cd] and Yangjun Xia [iD][a]

Solvent additives play an important role in optimizing the morphology of the photoactive layer and improving the photovoltaic performance of polymer solar cells (PSCs). However, the toxicity of common additives to the environment limits their further application in photovoltaic cells. Herein, a non-toxic green food additive, benzyl salicylate (BS), was introduced as a novel solvent additive into inverted PSCs based on ITO/ZnO/PTB7-Th:PC$_{71}$BM/MoO$_3$/Ag. Subsequently, the effect of BS on the photovoltaic performance was studied, and the best power conversion efficiency (PCE) of 9.43% was achieved when adding 2% BS into the photoactive layer of PSCs. Furthermore, the PSCs treated by 1–4% BS all exhibited good photovoltaic performance compared to that using 3% DIO (8.56%), which demonstrated that the universality was very strong. In addition, a good solubility for fullerenes was presented on BS like DIO, which was determined by atomic force microscopy and transmission electron microscopy. The water contact angle and time-off flight secondary ion mass spectroscopy results manifested that the good solubility of high-boiling-point additive BS to PC$_{71}$BM could boost the phase composition distribution at the surface and in the vertical direction. Thus, an efficient route for exciton dissociation and charge transfer could be formed when the PSC was processed *via* 2% BS, which could also be ascertained by space charge limited current, impedance spectroscopy. The present research findings provide useful information for realizing large-area PSC fabrication, where a greener non-toxic additive is always preferred.

Introduction

Polymer solar cells (PSCs) have become the most promising means to solve the global energy shortage issues, owing to their advantages of flexibility, light weight, low-cost, and roll-to-roll fabrication.[1–8] A lot of efforts have been devoted to research on PSCs, including the design of donors and acceptors (fullerene and non-fullerene), interface modification, and optimization of the photoactive layer, which have pushed the power conversion efficiencies (PCEs) up to 17%.[9–16] Among these strategies, optimizing the photoactive layer is the simplest way to further boost the photovoltaic performance.[17–24] The morphology of the optimal photoactive layer can allow forming good inter-penetrating networks and a favorable degree of phase separation, which is beneficial to realize efficient exciton dissociation and charge transport. Generally, the typical morphology optimization methods are divided into hot substrate annealing, solvent additives, solvent vapor annealing, and solvent flush.[25–29] High-boiling-point solvent additives, such as 1,8-diiodooctane (DIO), diphenyl ether (DPE), *N*-methyl pyrrolidone (NMP), and chloronaphthalene, could prolong the drying process of the photoactive layer to realize a favorable degree of phase separation, which has been proved to be one of the most practical ways to improve the photovoltaic performance.[30–33]

The high-boiling-point additive 1,8-diiodooctane (DIO) is regarded as the most commonly used solvent additive for the optimization of the photoactive layer. In the past few decades, photoactive layers of PSCs treated with DIO have achieved a notable improvement in the PCE.[34,35] Furthermore, DIO has

[a] School of Materials Science and Engineering, Lanzhou Jiaotong University, Lanzhou, 730070, P. R. China. E-mail: ljfpyc@163.com

[b] Shanghai Synchrotron Radiation Facility, Shanghai Advanced Research Institute, Chinese Academy of Sciences, 239 Zhang Heng Road, Pudong New District, Shanghai 201204, P. R. China

[c] Qingdao Institute of Bioenergy and Bioprocess Technology, Chinese Academy of Sciences, Qingdao 266101, P. R. China. E-mail: baoxc@qibebt.ac.cn

[d] Center for Ocean Mega-Science, Chinese Academy of Sciences, 7 Nanhai Road, Qingdao, 266071, China

† Electronic supplementary information (ESI) available. See DOI: 10.1039/c9tc06571g

‡ Jianfeng Li and Yufei Wang contributed equally to this work.

This journal is © The Royal Society of Chemistry 2020

J. Mater. Chem. C, 2020, **8**, 2483–2490 | **2483**

been certified to be much more soluble in fullerenes than most polymers, and the influence of DIO on PSCs has thus been widely studied.[36] DIO has a higher boiling point (bp) 332.5 °C than chlorobenzene (CB, 132 °C) and *o*-dichlorobenzene (180.5 °C). Thus, DIO can remain for a period of time after the host solvent CB is volatilized (polymer:fullerene casting CB solvent processed with DIO). The polymer phase is preferentially formed and as a result DIO can selectively dissolve fullerene, which can provide the fullerene phase a chance to rearrange in the photoactive layer, and thus an ideal photoactive layer can be formed.[37] The ideal photoactive layer requires a donor-rich anode and acceptor-rich cathode for inverted photovoltaic devices, which could realize more efficient charge transport and less recombination, corresponding to a higher fill factor (FF) and short circuit current density (J_{sc}). Therefore, it is important to study the composition (donor and acceptor) distribution for further understanding the influence of additives on the photoactive layer. Zhao *et al.* adjusted the gradient three-dimensional (3D) morphology of the photoactive layer by introducing different contents of DIO, and reported the PCEs of photovoltaic devices (PTB7:PC$_{71}$BM) could be increased from 6.79% to 7.67%.[38] Wang *et al.* probed the vertical concentration distribution of PTB7-Th:PC$_{71}$BM (after adding DIO) flushed with 2-chlorophenol, whereby a bottom-rich region of PC$_{71}$BM and upper-rich region of PTB7-Th were formed, which could boost the charge transport and reduce recombination.[39] Thus, PTB7-Th can be regarded as an ideal model for probing the influence of additives on the film-fullerene formation dynamics. Although high-boiling-point solvent additives (DIO, DPE, NMP) have excellent properties, the toxicity of these additives further limits their advances and use in large-scale production. A green additive butylamine was introduced by Tan *et al.*, where the P3HT:PCBM film exhibited a vertical phase segregation morphology.[40] Ye *et al.* used a food additive *o*-methylanisole as a solvent additive to realize similar crystalline properties and domain purity as the binary solvent (chlorobenzene and DIO), and a comparable photovoltaic performance was obtained.[41] Although there have been some reports on green additives, it is not clear how green additives adjust the vertical composition distribution.

In this work, a new type of green-food additive benzyl salicylate (BS) was introduced into inverted PSCs based on PTB7-Th:PC$_{71}$BM. BS is non-toxic, and can provide a possibility for use in large-scale industrial fabrication. Excellent photovoltaic performance (open circuit voltage (V_{oc}) of 0.80 V, short circuit density (J_{sc}) of 16.78 mA cm^{-2}, fill factor (FF) of 70.28%, and PCE of 9.43%) was obtained when the PSCs were processed with 2% BS, which was better than that with 3% DIO (8.56%). The high-boiling-point solvent additive BS, like DIO, can prolong the drying process and dissolve PC$_{71}$BM, resulting in a rearrangement between PTB7-Th and PC$_{71}$BM in the photoactive layer (as determined by atomic force microscopy (AFM) and transmission electron microscopy (TEM)). The water contact angle (WCA) and time-of-flight secondary ion mass spectroscopy (TOF-SIMS) results showed that PTB7-Th and PC$_{71}$BM were enriched on the top and the bottom region of

the photoactive layer, respectively, which could promote charge transport and reduce recombination.

Results and discussion

PSCs with various additives were assembled based on ITO/ZnO/PTB7-Th:PC$_{71}$BM/MoO$_3$/Ag. The related preparation process of the photovoltaic devices are presented in the ESI.† The photoactive layer consisted of PTB7-Th:PC$_{71}$BM (total concentration of 25 mg mL^{-1}, weight ratio of 1:1.5) dissolved in CB. The corresponding device architecture and chemical structures are shown in Fig. 1.

Photovoltaic performance

To probe the influence of the BS contents on the photovoltaic performance, the current density–voltage curves (J–V) of the PSCs with different volume ratios of BS (contrast to CB) and without the additive (w/o additives) were measured (Fig. S1, ESI†). The parameters of the photovoltaic performance are summarized in Table S1 (ESI†). A notable enhancement was observed, whereby the PCE was improved from 4.60% to 8.46% when 0.5% BS was added. With the increase in BS content from 0.5% to 5%, the PCE of the PSCs increased at first and then decreased. It was noted that the PCE achieved an optimal value of 9.43% when the PSCs were processed with 2% BS. Meanwhile, control inverted PSCs based on PTB7-Th:PC$_{71}$BM (adding 3% DIO) were fabricated and tested. The related J–V curves and parameters are also displayed in Fig. 1c and Table 1. The photovoltaic device with 3% DIO exhibited a PCE of 8.56%, a poor J_{sc} of 15.97 mA cm^{-2}, and a weak FF of 66.99% compared to the PSC with 2% BS. Interestingly, the photovoltaic performance of the PSCs with BS under small volume ranges (1–4%) were better than the devices with 3% DIO additive. Therefore, the utilization of the additives in a small varied range while maintaining a high PCE provides the possibility for large-scale industrial production. In addition, a large shunt resistance (R_{sh}) of
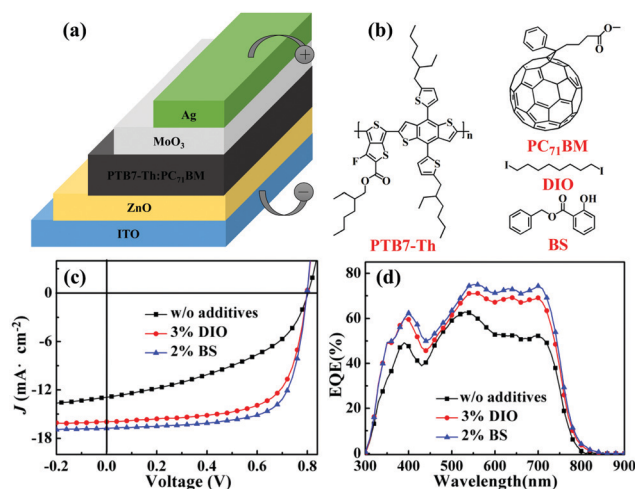

Fig. 1 (a) Device architecture, (b) chemical structures of PTB7-Th, PC$_{71}$BM, DIO, and BS, (c) J–V curves of the PSCs with different additives and (d) the corresponding EQE spectra.

2484 | *J. Mater. Chem. C*, 2020, **8**, 2483–2490

This journal is © The Royal Society of Chemistry 2020

Table 1 Parameters of photovoltaic devices with different additives

Additives	V_{oc}^{a} (V)	J_{sc}^{a} (mA cm^{-2})	FF^{a} (%)	PCE^{a} (%)	R_s (Ω cm^2)	R_{sh} (Ω cm^2)	J_{sc}/J_{sat} (%)
Without	0.80 ± 0.02	12.92 ± 0.44 (12.62)^b	44.47 ± 0.23	4.60 ± 0.21	10.11	238.10	81.15
3% DIO	0.80 ± 0.01	15.97 ± 0.31 (15.45)^b	66.99 ± 0.34	8.56 ± 0.15	3.94	792.85	93.87
2% BS	0.80 ± 0.01	16.78 ± 0.37 (16.43)^b	70.28 ± 0.16	9.43 ± 0.11	3.44	1059.95	94.91

^{a} Averaged photovoltaic values were calculated from 15 separate devices. ^{b} The values of J_{sc} were calculated from the EQE spectra.

1059.95 Ω cm^2 and small series resistance (R_s) of 3.44 Ω cm^2 were obtained for the PSC with 2% BS, indicating that the introduction of BS could boost the charge extraction and reduce the recombination rate,[42] thus wonderful J_{sc} and FF values were acquired. Furthermore, the external quantum efficiency (EQE) curves of the PSCs with different additives are given in Fig. 1d. A great improvement of the EQE spectra in the 500 to 700 nm range (as shown in Fig. 1b) was obtained with the introduction of the additives, which may be attributed to the greater light absorption and better phase separation between the PTB7-Th and PC$_{71}$BM. A small deviation (under 5%) of J_{sc} was calculated from J–V curves and EQE spectra, respectively, indicating that the J_{sc} values from J–V curves were credible.

Morphology research

It is not difficult to see that the advancement in PCE caused by the BS additive resulted from the higher J_{sc} and FF and benefited from the mechanism of the high-boiling-point additive DIO's ability to enhance the photovoltaic performance based on fullerene. Here, the high-boiling-point additive DIO could dissolve PCBM and prolong the drying process of the photoactive layer, which enabled the PCBM to have more time to rearrange, and thus an ideal morphology could be obtained.[43] Thus, atomic force microscopy (AFM) and transmission electron microscopy (TEM) measurements of PSCs under different conditions were performed to better illustrate the role of the BS additive on the morphology of the photoactive layer. The AFM height and phase images of the blend films with different additives are exhibited in Fig. 2a–f. As shown in Fig. 2d, a distinct PC$_{71}$BM aggregation was found for the PTB7-Th:PC$_{71}$BM film without any additive. Afterwards, the PC$_{71}$BM aggregation disappeared as the additives (3% DIO or 2% BS) were added into PTB7-Th:PC$_{71}$BM (as displayed in Fig. 2e and f), which indicated that the PC$_{71}$BM in the blend film could be dissolved with the assistance of the additives. Besides, the root-mean-square (RMS) values of the PTB7-Th:PC$_{71}$BM blend film under different conditions were 1.71 nm (w/o additives), 1.75 nm (3% DIO), and 1.67 nm (2% BS), respectively. A smoother surface and disappearance of PC$_{71}$BM was noted from the blend film with 2% BS, which could boost the exciton dissociation and form an effective path for the charges, thus leading to a high J_{sc} and FF.

TEM measurements of the blend films under different process conditions were carried out for further verifying that BS could dissolve PC$_{71}$BM. As shown in Fig. 2g–i, the PTB7-Th enrichment areas and PC$_{71}$BM enrichment areas were manifested as dark and bright regions, respectively. In the TEM
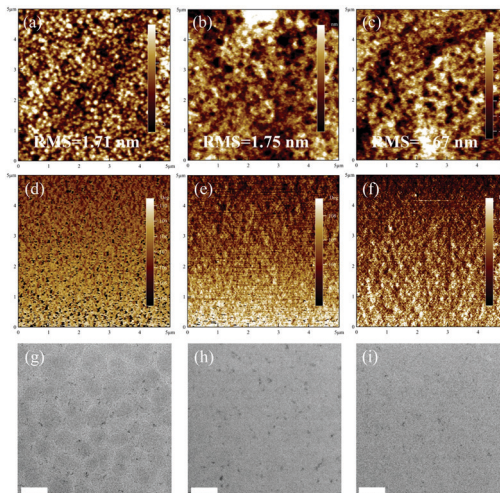

Fig. 2 The AFM height images (a–c), and the correlated phase images (d–f) of PTB7-Th:PC$_{71}$BM under different treatment conditions. TEM images of PTB7-Th:PC$_{71}$BM with different treatment conditions are shown in (g–i), and the scale bar was 200 nm. Note: (a, d and g) w/o additives, (b, e and h) 3% DIO, (c, f and i) 2% BS.

image (Fig. 2g) of PTB7-Th:PC$_{71}$BM without additives, an obvious PC$_{71}$BM aggregation could be observed. Then, the large PC$_{71}$BM aggregation disappeared when 3% DIO was added into the blend film, which resulted from the PC$_{71}$BM being dissolved under the role of DIO, and this is consistent with a previous report.[37] A similar result to the PTB7-Th:PC$_{71}$BM film with 3% DIO treatment was presented, where PC$_{71}$BM aggregation also disappeared for the blend film when adding 2% BS additive. Thus, a reasonable conclusion that BS can dissolve PC$_{71}$BM was confirmed, which could provide PC$_{71}$BM a chance to rearrange and induce an ideal morphology for exciton dissociation and charge transport.

To further investigate the influence of different solvent additives on the molecular stacking and aggregation of the active layer, grazing incidence wide-angle X-ray scattering (GIWAXS) was conducted and the results are illustrated in Fig. 3. As shown in Fig. 3a–c, the GIWAXS 2D patterns were alike with the different solvent additive treatments and this similarity is even clearer in the 1D profiles (Fig. 4d). The active layer under different treatment conditions showed two distinct peaks at $q = 0.30$ Å^{-1} and 1.32 Å^{-1}, which were caused by the (100) Bragg diffraction because of the lamellar packing of PTB7-Th and PC$_{71}$BM, respectively. However, the locations and intensities of those peaks were almost the same in the blend films under different conditions, indicating that the solvent additives did not have much effect on the crystallinity of the PTB7-Th:PC$_{71}$BM films.
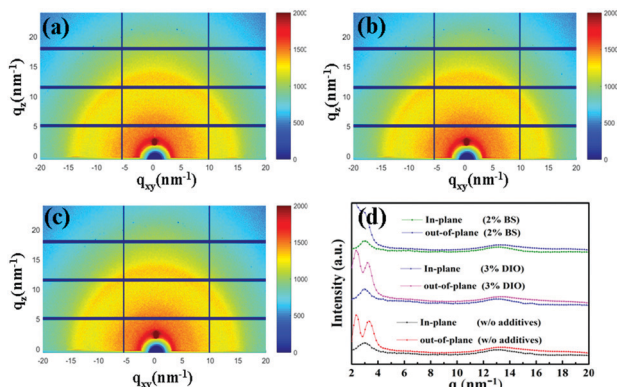
This journal is © The Royal Society of Chemistry 2020

J. Mater. Chem. C, 2020, **8**, 2483–2490 | **2485**

Fig. 3 2D GIWAXS images of PTB7-Th:PC$_{71}$BM blend films under different treatment conditions: (a) w/o additives, (b) with 3% DIO, (c) with 2% BS. (d) Integrated scattering profiles of the corresponding blend films.
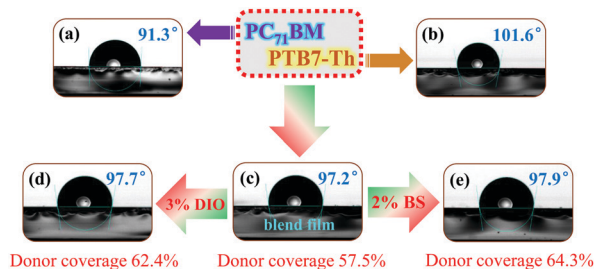

Fig. 4 WCA images of film: (a) neat PC$_{71}$BM, (b) neat PTB7-Th, (c) blend film. (d and e) WCA images of the blend film with the additives: (d) 3% DIO and (e) 2% BS.

Therefore, the results indicated that the improved device performance with the solvent additives did not result from the variation of the molecular packing of the blend films.

Phase-composition distribution

Although the high-boiling-point BS could dissolve PC$_{71}$BM and regulate the morphology of the active layers, the mechanism for the improvement of the photovoltaic performance is unclear. To further explore the ability of BS toward morphological regulation, water contact angle (WCA) measurements of the blend films under different conditions were tested for semi-quantitatively calculating the phase component (PTB7-Th and PC$_{71}$BM) content on the surface of the photoactive layer.[44] The WCA images of the neat PC$_{71}$BM film (91.3°), neat PTB7-Th film (101.6°), and blend film under different conditions (w/o additives, 3% DIO, 2% BS) are displayed in Fig. 4a. According to the Cassie–Baxter formula:[45]

$$\cos\theta = f\cos\theta_{PTB7\text{-}Th} + (1-f)\cos\theta_{PC_{71}BM} \qquad (1)$$

where $\theta_{PTB7\text{-}Th}$ and $\theta_{PC_{71}BM}$ represent the WCA values of the neat PTB7-Th film and neat PC$_{71}$BM film, respectively, θ denotes the WCA of the PTB7-Th:PC$_{71}$BM blend film, and f is the coverage fraction of PTB7-Th. The PTB7-Th coverage fraction of the blend film surface was determined by eqn (1), and the related results are shown in Table S2 (ESI†). Here, a 57.5% coverage fraction f was obtained for the blend film without any additive,

and then, f improved to 62.4% (3% DIO) and 64.3% (2% BS) with the introduction of additives, suggesting high-boiling-point additives (DIO and BS) can boost the surface fraction of PTB7-Th resulting from the morphology rearrangement that happens because DIO and BS can dissolve PC$_{71}$BM.

To further understand the effect of the additives on the vertical distribution of the phase components, TOF-SIMS measurements of the blend film with different additives were conducted. Since PTB7-Th contains the characteristic elements F and S atoms, which are not possessed by PC$_{71}$BM, we could analyze the distribution of PTB7-Th in the vertical direction of the active layer by detecting the yield distribution of F$^-$ and S$^-$ with the sputtering time. Therefore, the depth profiles of F$^-$ and S$^-$ in the blend films with different additives were obtained by TOF-SIMS measurements, as shown in Fig. 5a. It can be seen that a stronger F$^-$ signal could be obtained by the blend film with 3% DIO than the pristine film before the sputtering time reached 250 s, whereas the blend film without additives acquired intense signals of F$^-$. The reason for this result may be that the PC$_{71}$BM on the surface of the blend film migrated to the bottom with the assistance of 3% DIO (DIO can dissolve PC$_{71}$BM), while the content of PTB7-Th on the surface was relatively high, resulting in a stronger F$^-$ signal on the surface. Moreover, the phenomenon of PC$_{71}$BM migration for the blend film with 2% BS was more remarkable than for the blend film with 3% DIO, which was consistent with the results of the WCA measurements. Meanwhile, the top projection images of the F$^-$ yield distribution of the blend film with different additives are visually shown in Fig. 6a–c and e, f when the sputtering time reached 20 s and 600 s, respectively. In addition, the phenomenon of PC$_{71}$BM migration could be further proved by the distribution results of the S$^-$ signal yield, as shown in Fig. 5b and Fig. S2 (ESI†). The result showed that the rearranged phase components caused by PC$_{71}$BM migration produced a high content distribution of PTB7-Th on the surface, which may boost exciton dissociation and charge transport (holes were especially noticeable), and thus a high FF and J_{sc} were obtained.

Charge generation, transport, and recombination

To research the effect of the rearranged phase components distribution on the photocurrent properties, the photocurrent density (J_{ph}) versus effective voltage (V_{eff}) and corresponding exciton dissociation rate ($P(E,T)$) versus effective voltage (V_{eff}) curves of the PSCs with different additives were plotted and
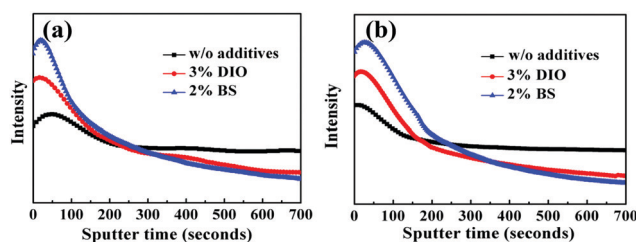

Fig. 5 TOF-SIMS signals of the blend film under different treatment conditions: (a) F$^-$ signals, (b) S$^-$ signals.
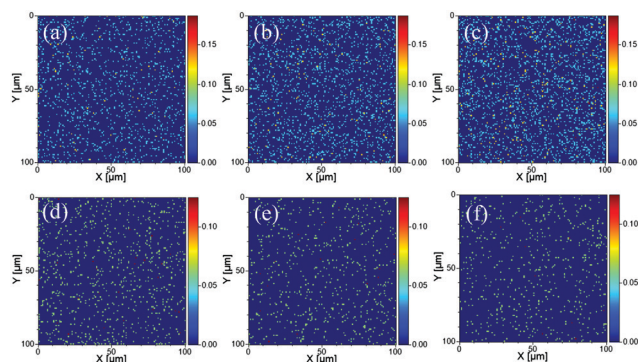
Fig. 6 Top projection images of the F⁻ content of the blend film with additives treatment under TOF-SIMS measurement at different sputtering times: (a–c) 20 s and (d–f) 600 s, (a and d) w/o additives, (b and e) 3% DIO, (c and f) 2% BS.

displayed in Fig. 7a and Fig. S3 (ESI†), respectively. J_{ph} can be acquired from the formula: $J_{ph} = J_{light} - J_{dark}$, where J_{light} and J_{dark} denote the current density under illumination and dark conditions, respectively. V_{eff} can be obtained from an equation $V_{eff} = V_0 - V_{appl}$, where V_0 represents the voltage of J_{light} equal to J_{dark} and V_{appl} is the applied voltage around the PSC.[46–50] Remarkably, the J_{ph}–V_{eff} curves exhibited two different regions: a linear growth region ($V_{eff} < 0.1$ V) and saturated region ($V_{eff} > 1$ V). The J_{ph} linearly improved with V_{eff} in the linear growth region, while J_{ph} approached a saturated value with V_{eff} increasing in the saturated region. Thus, $P(E,T)$ could be determined via the equation: $P(E,T) = J_{ph}/J_{sat}$, where J_{sat} is the saturated current density.[51–54] At $V_{eff} = 3$ V, the J_{sat} values of the photovoltaic devices were 15.76 (w/o additives), 17.01 (3% DIO), and 17.68 mA cm⁻² (2% BS), respectively. The corresponding $P(E,T)$ values (listed in Table 1) were 81.15%, 93.87%, and 94.91%, which indicated that the formed enriched regions (PTB7-Th and PC₇₁BM) at the photoactive surface after adding the additives could facilitate exciton dissociation at the
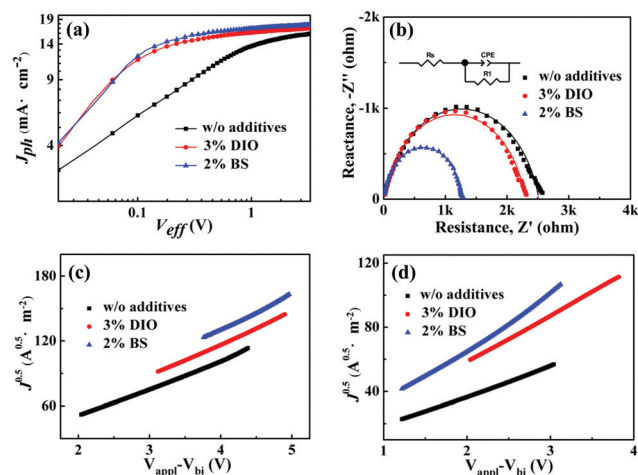
interface (PTB7-Th and PC₇₁BM) and reduce recombination. It was noted that the formed enriched regions of the PSCs with 2% BS were more notable than the PSCs with 3% DIO, thus a higher J_{sc} and FF could be forecast.

The performance enhancement caused by the phase components rearrangement of the photoactive layer can be reflected by the improvement of the carrier transport dynamics. Therefore, impedance spectroscopy (IS) of photovoltaic devices under different conditions was performed, characterized at V_{oc} (0.80 V) with a small amplitude (0.5 mV) and frequency ranging from 100 Hz to 1 MHz in the dark. Typical Nyquist plots of resistance (Z') versus frequency (Fig. S4a, ESI†) and reactance (Z'') versus frequency (Fig. S4b, ESI†) were performed and are presented in Fig. 7b. As shown in Fig. 7b, the symbol represents the original data and the line denotes the fitting data using an equivalent circuit. The equivalent circuit is given in the insert of Fig. 7b, including the constant phase element (CPE), parallel resistance R_1, and series resistance R_s, where CPE represents a non-ideal capacitor with an inhomogeneous interface, consisting of CPE-T and CPE-P, CPE-T denotes a capacitance value, and CPE-P is a trend factor in contrast to an ideal capacitor. The CPE exhibits an ideal capacitor behavior when the value of CPE-P is 1, while CPE is a capacitor with defects when CPE-P is below 1. The R_s in the equivalent circuit is related to the series resistor loss consisted of the interface modification layer (ZnO and MoO₃) and blend film, which was reflected by the intercept of the Nyquist plots on the Z' axis left. However, the right intercept (Nyquist plots on the Z' axis) was reduced significantly with the employment of 2% BS, which was relevant to the higher J_{sc}.[55] In addition, R_1 is relevant to the recombination process existing in PSCs. The fitting parameters of IS using the equivalent circuit are listed in Table 2. A high extent of fitting with a small error rate (below 14%) could be observed from Fig. 7b and Table 2, which indicated that the fitting data was reliable. The R_s of all the PSCs exhibited almost similar values (Table 2), which was the related to the identical device structure. CPE-P was improved from 0.85 to 0.94 with using 2% BS, indicating that the blend film with 2% BS formed a homogeneous interface stemming from the rearrangement of the morphology, which was consistent with the AFM results.[22] In addition, R_1 related to the recombination process was reduced from 2506 (w/o additives) to 1260 Ω (2% BS), which showed that the rearranged structure (PTB7-Th enriched upper region) caused by 2% BS could reduce the charge recombination.

To further comprehend the influence of the additives on the photovoltaic performance, hole-only and electron-only devices were fabricated and tested with ITO/PEDOT:PSS/PTB7-Th:PC₇₁BM/MoO₃/Ag and ITO/ZnO/PTB7-Th:PC₇₁BM/PFN/Al, respectively. The fitting J–V curves of the hole-only and electron-only devices are

Fig. 7 (a) The photocurrent vs. effective voltage curves and (b) Nyquist plots curve, fitting J–V curves of (c) hole-only device and (d) electron-only device for PSCs with diverse additives processed.

Table 2 Parameters used for the fitting of the impedance spectra

Additives	R_s (Ω)	R_1 (Ω)	CPE1-T (F)	CPE1-P	Error (%)
w/o	8.89	2506	2.53×10^{-8}	0.85	0.38–13.23
3% DIO	10.94	2283	2.49×10^{-8}	0.87	0.40–9.42
2% BS	10.37	1260	7.87×10^{-9}	0.94	0.31–7.74

This journal is © The Royal Society of Chemistry 2020

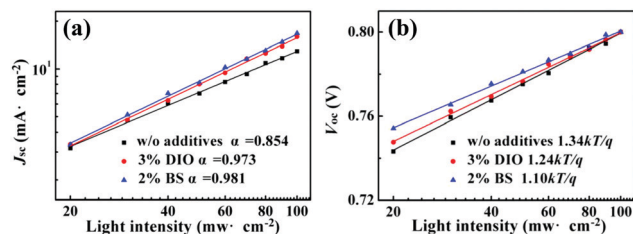J. Mater. Chem. C, 2020, 8, 2483–2490 | 2487

Fig. 8 The J_{sc} vs. P_{light} curves (a) and V_{oc} vs. P_{light} curves (b).

presented in Fig. 7c and d, and the related parameters were calculated according to the Mott–Gurney law and are listed in Table S3 (ESI†).[56–58] The hole-mobility values of the PSCs with different treatment conditions were 2.18×10^{-4} (w/o additives), 2.75×10^{-4} (3% DIO), 3.62×10^{-4} (2% BS) $cm^2 V^{-1} s^{-1}$, respectively, while the values for electron mobility were 1.15×10^{-4}, 3.06×10^{-4}, and 3.60×10^{-4} $cm^2 V^{-1} s^{-1}$, respectively. The mobility values (holes and electrons) of the PSCs with the additives were significantly improved, which could be related to the extent of the vertical phase composition distribution. A remarkable vertical phase composition distribution (PTB7-Th enriched upper) was obtained when 2% BS was used in the PSCs, which could induce effective hole transport and high hole mobility. Meanwhile, the balanced carrier mobility ratio was acquired in the presence of 2% BS, which could partly illustrate the reason for the high FF and J_{sc}.

To make a thorough inquiry into the actions of the BS additive on charge recombination, the relationships of J_{sc} and V_{oc} versus the light intensity (I_{light}) were measured (Fig. 8). Here, J_{sc} and I_{light} obey the relationship expression:

$$J_{sc} \propto I_{light}^{\alpha} \qquad (2)$$

where α denotes a value for the exponential factor.[59] When α approaches 1, photogenerated carriers in short circuits can be collected by electrodes before recombination, which indicates that bimolecular recombination is greatly suppressed.[60,61] These α values of the PSCs with different treatment conditions were 0.854 (w/o additives), 0.973 (3% DIO), and 0.981 (2% BS), respectively. A larger α of 0.981 was obtained for the PSC with 2% BS, which indicated the rearranged morphology (caused by 2% BS) could reduce the bimolecular recombination, thus a higher FF and J_{sc} were realized. The results of the J_{sc}–I_{light} curves were consistent with the V_{oc}–I_{light} diagram as shown in Fig. 8b. Here, V_{oc} and I_{light} satisfy the relation formula:

$$V_{oc} \propto \frac{nkT}{q} \ln(I_{light}) \qquad (3)$$

where q and T denote the element charge and Kelvin temperature, respectively, and k and n are the Boltzmann constant and the slope, respectively. The slope n value can give an indication of the recombination property under an open-circuit condition. The bimolecular recombination becomes a major recombination process when n is close to 1, while trap-assisted recombination occupies the dominant position in the recombination process when n approaches 2.[62,63] The n values of the PSCs were 1.34 (w/o additives), 1.24 (3% DIO), and 1.10 (2% BS), respectively. Remarkably, bimolecular recombination was the primary

recombination process in the PSCs and the employment of additives (3% DIO or 2% BS) could reduce the bimolecular recombination, and here, the effect of the BS additive was more significant.

Conclusion

In this work, a new green food additive, named benzyl salicylate (BS), was successfully introduced into PSCs based on PTB7-Th:PC$_{71}$BM. As a high-boiling-point (up to 335 °C) additive, BS exhibited a similar property that had an ability to dissolve PC$_{71}$BM as DIO. The best PCE of 9.43% was acquired for the PSCs with 2% BS, better than the traditional PSC devices (adding 3% DIO). In addition, the PSCs with a range from 1% to 4% BS could also achieve good photovoltaic performance compared to that of the PSCs using 3% DIO, indicating BS possesses a universal applicability in PSCs. The improved performance on the PSCs with 2% BS was attributed to the optimal phase composition distribution, whereby a PTB7-Th enriched region was formed on the top surface of the blend films, where the PTB7-Th enriched region formed by the 2% BS treated blend film was more significant than that of 3% DIO, which could reduce recombination and boost charge transport. This hypothesis was certified by SCLC, impedance spectroscopy, thus a higher FF and J_{sc} could be observed. The work indicates that the non-toxic green solvent additive BS can become a promising method for boosting the photovoltaic performance of PSCs. The finding provides useful information for realizing large-area PSC fabrication, where a greener non-toxic additive is always preferred.

Conflicts of interest

There are no conflicts to declare.

Acknowledgements

Notes and references

1 K. Gao, Z. Zhu, B. Xu, S. B. Jo, Y. Kan, X. Peng and A. K. Y. Jen, *Adv. Mater.*, 2017, **29**, 1703980.

2 X. Wang, Z. Du, K. Dou, H. Jiang, C. Gao, L. Han and R. Yang, *Adv. Energy Mater.*, 2019, **9**, 1802530.

3 X. Li, Z. Liang, H. Wang, S. Qiao, Z. Liu, H. Jiang, W. Chen and R. Yang, *J. Mater. Chem. A*, 2020, DOI: 10.1039/C9TA10610C.

4 T. Liu, L. Huo, S. Chandrabose, K. Chen, G. Han, F. Qi, X. Meng, D. Xie, W. Ma, Y. Yi, J. M. Hodgkiss, F. Liu, J. Wang, C. Yang and Y. Sun, *Adv. Mater.*, 2018, **30**, 1707353.

2488 | *J. Mater. Chem. C*, 2020, **8**, 2483–2490

This journal is © The Royal Society of Chemistry 2020

5 K. Gao, S. B. Jo, X. Shi, L. Nian, M. Zhang, Y. Kan, F. Lin, B. Kan, B. Xu, Q. Rong, Q. Rong, L. Shui, F. Liu, X. Peng, G. Zhou, Y. Cao and A. K. Y. Jen, *Adv. Mater.*, 2019, **31**, 1807842.

6 X. Bao, Y. Zhang, J. Wang, D. Zhu, C. Yang, Y. Li, C. Yang, J. Xu and R. Yang, *Chem. Mater.*, 2017, **29**, 6766.

7 W. Chen, G. Huang, X. Li, Y. Li, H. Wang, H. Jiang, Z. Zhao, D. Yu, E. Wang and R. Yang, *ACS Appl. Mater. Interfaces*, 2019, **11**, 33173.

8 K. Gao, L. Li, T. Lai, L. Xiao, Y. Huang, F. Huang, J. Peng, Y. Cao, F. Liu, T. P. Russell, R. A. Janssen and X. Peng, *J. Am. Chem. Soc.*, 2015, **137**, 7282.

9 T. Duan, H. Tang, R. Liang, J. Lv, Z. Kan, R. Singh, M. Kumar, Z. Xiao, S. Lu and F. Laquai, *J. Mater. Chem. A*, 2019, **7**, 2541–2546.

10 W. Chen, W. Shen, H. Wang, F. Liu, L. Duan, X. Xu, D. Zhu, M. Qiu, E. Wang and R. Yang, *Dyes Pigm.*, 2019, **166**, 42.

11 J. Li, N. Wang, Y. Wang, Z. Liang, Y. Peng, C. Yang, X. Bao and Y. Xia, *Sol. Energy*, 2020, **196**, 168.

12 L. An, J. Tong, C. Yang, X. Zhao, X. Wang and Y. Xia, *Polym. Int.*, 2020, **69**, 192.

13 H. Tang, T. Xu, C. Yan, J. Gao, H. Yin, J. Lv, R. Singh, M. Kumar, T. Duan, Z. Kan, S. Lu and G. Li, *Adv. Sci.*, 2019, **6**, 1901613.

14 H. Chen, D. Hu, Q. Yang, J. Gao, J. Fu, K. Yang, H. He, S. Chen, Z. Kan, T. Duan, C. Yang, J. Ouyang, Z. Xiao, K. Sun and S. Lu, *Joule*, 2019, **3**, 3034.

15 H. Tan, Y. Long, J. Zhang, J. Zhu, J. Yang, J. Yu and W. Zhu, *Dyes Pigm.*, 2019, **162**, 797.

16 J. Lv, Y. Feng, J. Fu, J. Gao, R. Singh, M. Kumar, M. Kim, H. Tang, S. Lu, W. Zhang, I. McCulloch, J. Li and Z. Kan, *Sol. RRL*, 2019, 1900403.

17 X. Kong, H. Lin, X. Du, L. Li, X. Li, X. Chen, C. Zheng, D. Wang and S. Tao, *J. Mater. Chem. C*, 2018, **6**, 9691–9702.

18 L. Li, H. Lin, X. Kong, X. Du, X. Chen, L. Zhou, S. Tao, C. Zheng and X. Zhang, *Nanoscale*, 2018, **10**, 9971–9980.

19 X. Du, X. Lu, J. Zhao, Y. Zhang, X. Li, H. Lin, C. Zheng and S. Tao, *Adv. Funct. Mater.*, 2019, **29**, 1902078.

20 H. Tan, X. Zheng, J. Zhu, J. Yu and W. Zhu, *J. Mater. Chem. C*, 2019, **7**, 13301–13306.

21 W. Peng, G. Zhang, L. Shao, C. Ma, B. Zhang, W. Chi, Q. Peng and W. Zhu, *J. Mater. Chem. A*, 2018, **6**, 24267.

22 C. Duan, K. Gao, F. J. M. Colberts, F. Liu, S. C. J. Meskers, M. M. Wienk and R. A. J. Janssen, *Adv. Energy Mater.*, 2017, **7**, 1700519.

23 Z. Luo, C. Sun, S. Chen, Z.-G. Zhang, K. Wu, B. Qiu, C. Yang, Y. Li and C. Yang, *Adv. Energy Mater.*, 2018, **8**, 1800856.

24 J. Tong, L. An, J. Lv, P. Guo, X. Wang, C. Yang and Y. Xia, *Polymers*, 2019, **11**, 12.

25 S. Guo, J. Ning, V. Körstgens, Y. Yao, E. M. Herzig, S. V. Roth and P. Müller-Buschbaum, *Adv. Energy Mater.*, 2014, **5**, 1401315.

26 K. Gao, J. Miao, L. Xiao, W. Deng, Y. Kan, T. Liang, C. Wang, F. Huang, J. Peng, Y. Cao, F. Liu, T. P. Russell, H. Wu and X. Peng, *Adv. Mater.*, 2016, **28**, 4727.

27 K. Gao, W. Deng, L. Xiao, Q. Hu, Y. Kan, X. Chen, C. Wang, F. Huang, J. Peng, H. Wu, X. Peng, Y. Cao, T. P. Russell and F. Liu, *Nano Energy*, 2016, **30**, 639.

28 C. R. McNeill, J. J. M. Halls, R. Wilson, G. L. Whiting, S. Berkebile, M. G. Ramsey, R. H. Friend and N. C. Greenham, *Adv. Funct. Mater.*, 2008, **18**, 2309.

29 W. Wang, L. Song, D. Magerl, D. M. González, V. Körstgens, M. Philipp, J. F. Moulin and P. Müller-Buschbaum, *Adv. Funct. Mater.*, 2018, **28**, 1800209.

30 C. Liu, X. Hu, C. Zhong, M. Huang, K. Wang, Z. Zhang, X. Gong, Y. Cao and A. J. Heeger, *Nanoscale*, 2014, **6**, 14297.

31 X. Guo, C. Cui, M. Zhang, L. Huo, Y. Huang, J. Hou and Y. Li, *Energy Environ. Sci.*, 2012, **5**, 7943.

32 Y. Zheng, T. Goh, P. Fan, W. Shi, J. Yu and A. D. Taylor, *ACS Appl. Mater. Interfaces*, 2016, **8**, 15724.

33 D. Zhu, X. Bao, D. Ouyang, J. Wang, X. Yuan, Q. Wang, D. Zhou, S. Wen and R. Yang, *Nano Energy*, 2017, **40**, 495.

34 Z. He, C. Zhong, X. Huang, W. Y. Wong, H. Wu, L. Chen, S. Su and Y. Cao, *Adv. Mater.*, 2011, **23**, 4636.

35 W. Zhang, Y. Wu, Q. Bao, F. Gao and J. Fang, *Adv. Energy Mater.*, 2014, **4**, 1400359.

36 K. R. Graham, P. M. Wieruszewski, R. Stalder, M. J. Hartel, J. Mei, F. Reynolds and J. R. So, *Adv. Funct. Mater.*, 2012, **22**, 4801.

37 F. Liu, W. Zhao, J. R. Tumbleston, C. Wang, Y. Gu, D. Wang, A. L. Briseno, H. Ade and T. P. Russell, *Adv. Energy Mater.*, 2014, **4**, 1301377.

38 L. Zhao, S. Zhao, Z. Xu, Q. Yang, D. Huang and X. Xu, *Nanoscale*, 2015, **7**, 5537.

39 Y. Wang, H. Zhu, Z. Shi, F. Wang, B. Zhang, S. Dai and Z. Tan, *J. Mater. Chem. A*, 2017, **5**, 2319.

40 L. Tan, P. Li, Q. Zhang, R. L. Izquierdo, M. Chaker and D. Ma, *ACS Appl. Mater. Interfaces*, 2018, **10**, 6498.

41 L. Ye, Y. Xiong, H. Yao, A. Gadisa, H. Zhang, S. Li, M. Ghasemi, N. Balar, A. Hunt, B. T. O'Connor, J. Hou and H. Ade, *Chem. Mater.*, 2016, **28**, 7451.

42 J. Li, Y. Wang, Z. Liang, N. Wang, J. Tong, C. Yang, X. Bao and Y. Xia, *ACS Appl. Mater. Interfaces*, 2019, **11**, 7022.

43 S. Gao, W. Wang, E. M. Heizig, A. Naumann, G. Tainter, J. Perlich and P. Müller-Buschbaum, *ACS Appl. Mater. Interfaces*, 2017, **9**, 3740.

44 D. M. Huang, S. A. Mauger, S. Friedrich, S. J. George, D. Dumitriu-LaGrange, S. Yoon and A. J. Moule, *Adv. Funct. Mater.*, 2011, **21**, 1657.

45 A. B. D. Cassie and S. Baxter, Wettability of Porous Surfaces, *Trans. Faraday Soc.*, 1944, **40**, 546.

46 L. Lu, T. Xu, W. Chen, E. S. Landry and L. P. Yu, *Nat. Photonics*, 2014, **8**, 716.

47 X. Wang, K. Dou, B. Shahid, Z. Liu, Y. Li, M. Sun, N. Zheng, X. Bao and R. Yang, *Chem. Mater.*, 2019, **31**, 6163.

48 Z. Liang, J. Tong, H. Li, Y. Wang, N. Wang, J. Li, C. Yang and Y. Xia, *J. Mater. Chem. A*, 2019, **7**, 15841.

49 T. Liu, Z. Luo, Q. Fan, G. Zhang, L. Zhang, W. Gao, X. Guo, W. Ma, M. Zhang, C. Yang, Y. Li and H. Yan, *Energy Environ. Sci.*, 2018, **11**, 3275.

50 L. Xiao, T. Liang, K. Gao, T. Lai, X. Chen, F. Liu, T. P. Russell, F. Huang, X. Peng and Y. Cao, *ACS Appl. Mater. Interfaces*, 2017, **9**(35), 29917.

51 Y. Wang, Z. Liang, J. Qin, J. Tong, P. Guo, X. Cao, J. Li and Y. Xia, *IEEE J. Photovolt.*, 2019, **9**, 1678.

52 T. Liu, W. Gao, G. Zhang, L. Zhang, J. Xin, W. Ma, C. Yang, H. Yan, C. Zhan and J. Yao, *Sol. RRL*, 2019, **3**, 1800376.

53 K. Gao, B. Xu, C. Hong, X. Shi, H. Liu, X. Li, L. Xie and A. K.-Y. Jen, *Adv. Energy Mater.*, 2018, **8**, 1800809.

54 V. D. Mihailetchi, L. J. A. Koster, J. C. Hummelen and P. W. M. Blom, *Phys. Rev. Lett.*, 2004, **93**, 216601.

55 E. Yao, C. Chen, J. Gao, Y. Liu, Q. Chen, M. Cai, W. C. Hsu, Z. Hong, G. Li and Y. Yang, *Sol. Energy Mater. Sol. Cells*, 2014, **130**, 20.

56 C. Melzer, E. J. Koop, V. D. Mihailetchi and P. W. M. Blom, *Adv. Funct. Mater.*, 2004, **14**, 865.

57 M. Y. Chiu, U. Jeng, M. S. Su and K. H. Wei, *Macromolecules*, 2010, **43**, 428.

58 J. Li, Z. Liang, Y. Wang, H. Li, J. Tong, X. Bao and Y. Xia, *J. Mater. Chem. C*, 2018, **6**, 11015.

59 Y. Wang, B. Wu, Z. Wu, Z. Lan, Y. Li, M. Zhang and F. Zhu, *J. Phys. Chem. Lett.*, 2017, **8**, 5264.

60 S. Wang, Z. Li, X. Xu, G. Zhang, Y. Li and Q. Peng, *Adv. Mater. Interfaces*, 2019, **6**, 1801480.

61 Y. Wang, Z. Liang, X. Li, J. Qin, M. Ren, C. Yang, X. Bao, Y. Xia and J. Li, *J. Mater. Chem. C*, 2019, **7**, 11152.

62 A. K. K. Kyaw, D. H. Wang, V. Gupta, W. L. Leong, L. Ke, G. C. Bazan and A. J. Heeger, *ACS Nano*, 2013, **7**, 4569.

63 J. Wan, X. Xu, G. Zhang, Y. Li, K. Feng and Q. Peng, *Energy Environ. Sci.*, 2017, **10**, 1739.